A Novel Hybrid Modular Three-Level Shunt Active Power Filter

Yong Wang, *Member, IEEE*, Jialong Xu, Ling Feng, *Student Member, IEEE*, and Chengmin Wang

***Abstract*—Shunt active power filters (SAPF) are employed to improve power quality by injecting compensating harmonic current. The modular SAPF offers many new capabilities that are otherwise unavailable by the conventional SAPF, such as high crest factor compensating current and fast dynamic response. However, there are still challenges that are needed to be addressed, such as resonance and stability issues associated with the modular SAPF. To investigate these issues, this paper first presents a mathematical model for conventional modular SAPF system. Based on the mathematical analysis, a new hybrid three-level modular SAPF is presented that is composed of two types of modules, each with different current carrying capacities, *LCL* filter parameters, and switching frequencies. The proposed hybrid system provides a wider current tracking bandwidth and fast dynamic response as compared to the present modular SAPF. A novel self-adaptive active damping strategy is proposed that effectively suppresses resonance and coupling between modules. Mathematical analysis and experimental results have been used to verify the proposed system.**

***Index Terms*—Hybrid, modular, modeling, shunt active power filter (SAPF), three level.**

I. Introduction

With an increase in penetration of nonlinear loads throughout the power distribution system, current harmonic pollution at the grid side is growing. The increasing number of higher order harmonics causes a series of problems, including voltage and current stresses, electromagnetic interference, and power transmission losses [1], [2]. Accordingly, passive and active harmonic mitigation techniques have been a major focus of research in recent years [3], [4]. Shunt Active Power Filters (SAPF) are used to mitigate harmonics at the load end by injecting a compensating harmonic current equal in magnitude and opposite in phase to that being drawn by nonlinear loads applied [5]–[9].

Essentially, the SAPF behaves as a grid-tied inverter but supplies higher order harmonics current with higher current crest factor and higher current slew rate [10].

Manuscript received August 1, 2017; revised October 2, 2017; accepted November 7, 2017. Date of publication November 12, 2017; date of current version June 22, 2018. This work was supported by the National Natural Science Foundation of China through Project 51577118. Recommended for publication by Associate Editor Y. Xue. *(Corresponding author: Yong Wang.)*

The authors are with the Department of Electrical Engineering, Shanghai Jiao Tong University, Shanghai 200240, China (e-mail: wangyong75@sjtu.edu.cn; xujialongxc@foxmail.com; feng_ling@foxmail.com; wangchengmin@sjtu.edu.cn).

Color versions of one or more of the figures in this paper are available online at http://ieeexplore.ieee.org.

Digital Object Identifier 10.1109/TPEL.2017.2772811

The modular or parallel SAPF discussed in [11]–[15] is an improvement over the conventional SAPF. Given high crest factor and slew rate of the compensating current it can produce, the modular SAPF arguably provides the more effective solution to harmonic distortion in contrast to the conventional centralized SAPF structure. Enhanced performance can be observed especially in terms of tracking precision and dynamic response, since the compensating current evenly distributed between multiple modules. However, it will be later demonstrated through mathematical modeling in Section II, that it is difficult for the conventional structure of modular or parallel SAPF to reach an optimal balance between fast dynamic response and stable control performance.

The modular SAPF structure is very similar to that of parallel inverters. The coupling and resonance between inverters are major areas of research that have been well addressed for parallel inverters [16]–[22]. Modeling of parallel inverters, theoretical investigation of resonance, and interactions between parallel inverters have been discussed in [16]–[18]. It is concluded that the resonance between inverters is greatly influenced by output filter inductance and grid impedance. Therefore, conventionally, the resonance is suppressed by the *LCL* filter inductance regulation or structure design as those in [19] and [20]. In recent years, active damping has been extensively investigated to improve the conversion efficiency and current tracking precision. J. He *et al.* have presented active resonance suppressing strategies by regulating the control laws and applying grid feed-forward control scheme [21], [22].

Similar to conventional parallel sine wave inverters, the resonance suppression and control stability are the most important issues with SAPF. Two simple resonance suppression schemes are suggested in [14], the first method decreases repetitive control intensity at the cost of decreased compensation precision, whereas the second method aims to strengthen passive damping approach through addition of a damping resistor at the cost of a higher power loss. Similar issues have been addressed in [15] for parallel SAPF which shows that increasing the inductance and decreasing the proportional gain in PR controllers is effective to suppress resonance conditions.

The hardware structural features and dynamic response capabilities of SAPF are not fully discussed in [11]–[15], in which modular or parallel SAPFs have been essentially treated as parallel sine wave inverters. The resonance suppression methods developed for SAPF are limited to passive damping schemes. However, it should be noted that harmonic compensating current error tracking of SAPF differs notably from the output error

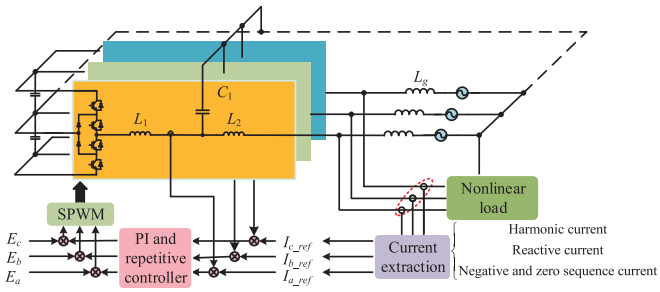

Fig. 1. General structure of three-level SAPF.

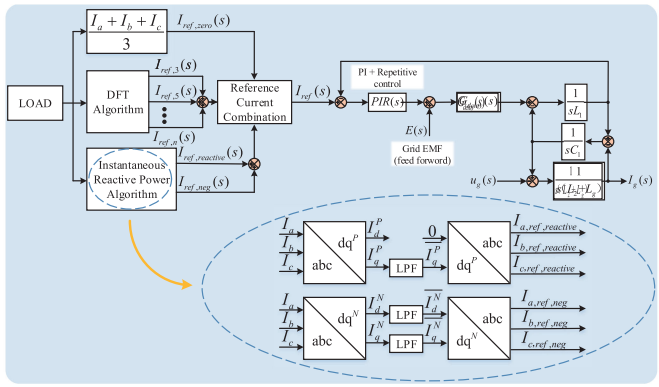

Fig. 2. Control diagram of modular SAPF.

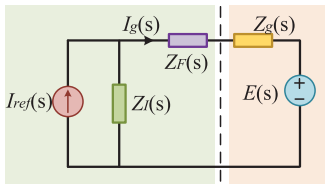

Fig. 3. Proposed single SAPF model in this paper.

tracking of conventional sine wave inverters, especially in terms of stability and dynamic response. The presence of higher order harmonics up to the 50th order in SAPF output translates into a higher crest factor in current. Therefore, the SAPF requires faster dynamic response and greater control bandwidth. Due to the aforementioned issues, the filter inductance for SAPF is usually designed to be much less than that of a conventional sine wave inverter. The lower filter inductance poses a greater risk of the resonance condition between parallel SAPF modules while also reducing the margin for resonance suppression by active and passive methods.

Given their fundamental differences from the parallel sine wave inverters, it is more difficult to arrive at a tradeoff between resonance suppression and dynamic response ability in modular SAPF. Therefore, neither of the active or passive resonance suppression methods can be directly utilized from conventional inverters as shown in [19]–[22].

This paper presents capabilities to address aforementioned issues associated with modular SAPF. First, a simplified mathematical model for a generalized three-level modular SAPF that includes a current controller, grid impedance, and active damping schemes is developed. Based on the mathematical analysis, we further propose a hybrid three-level modular SAPF system that is composed of two kinds modules with capacities of 100 A and 50 A, respectively. The 50-A module has lower *LCL* filter parameters and higher switching frequency to compensate harmonics of orders higher than 13th, and the 100-A module has larger *LCL* parameters and lower switching frequency to address the harmonics of lower order. Last, a novel self-adaptive active damping strategy is proposed and implemented for the modular SAPF to suppress resonance current between modules. The mathematical analysis and test results demonstrate that the proposed resonance control strategy can improve the compensating bandwidth and stability along with fast and precise harmonics tracking ability.

II. Modeling of Three-Level Modular SAPF

A. Modeling of a Single Three-Level SAPF

SAPF is essentially a controlled current source with output current feedback control. Every SAPF module is connected to the grid through a *LCL* filter as shown in Fig. 1. L_1, L_2, C, and L_g represent SAPF side inductor, grid side inductor, filter capacitor, and grid impedance, respectively.

The control scheme of a single SAPF is shown in Fig. 2. Although the reference current can be contributed by harmonic currents, reactive power, and unbalance (negative and zero sequence components) in the load, this paper mainly focuses on harmonic currents compensation. Harmonics are obtained by the selective harmonic detection algorithm based on discrete Fourier transform. $I_{\rm ref}$ represents the reference current, $u_g(s)$ is the grid voltage, and $E(s)$ is the feed-forward value of $u_g(s)$. The feedback control of the current loop is realized in *A-B-C* axis by a repetitive controller in parallel with a PI controller.

According to the control diagram in Fig. 2, the transfer function of the output current to the reference current reads

$$\begin{aligned} I_g(s) = &\{\mathrm{PIR}(s)G_{\rm delay}(s)I_{\rm ref}(s) - [s^2L_1C_1 \\ &+ sC_1\mathrm{PIR}(s)G_{\rm delay}(s) - G_{\rm delay}(s) + 1]E(s)\}/ \\ &[s^2C_1(L_2+L_g)\mathrm{PIR}(s)G_{\rm delay}(s) + s(L_1+L_2+L_g) \\ &- sL_gG_{\rm delay}(s) + \mathrm{PIR}(s)G_{\rm delay}(s) + s^3L_1C_1(L_2+L_g)] \end{aligned} \tag{1}$$

where $I_g(s)$ represents output current, $\mathrm{PIR}(s)$ is the transfer function of the PI and the repetitive controller used, and $G_{\rm delay}$ represents the delay due to system sampling, calculation, and transmission [23].

Fig. 3 shows the simplified, single three-level SAPF model proposed in this paper used to construct the modular system. The impedance averaging model and small signal linearization techniques have been used considering the difference of SAPF from the sine wave inverter models as presented in [24] and [25]. The proposed model can be divided into two parts: the current source inverter and the grid. The current source inverter is composed of the reference current $I_{\rm ref}(s)$, filter impedance $Z_F(s)$, and parallel output impedance $Z_I(s)$ introduced through

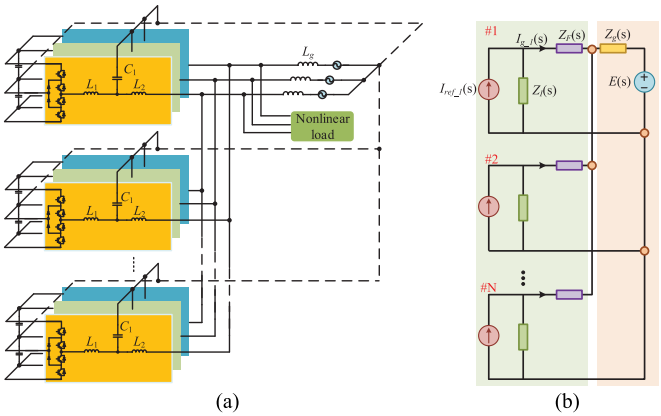

Fig. 4. Parallel structure of modular three-level SAPF.

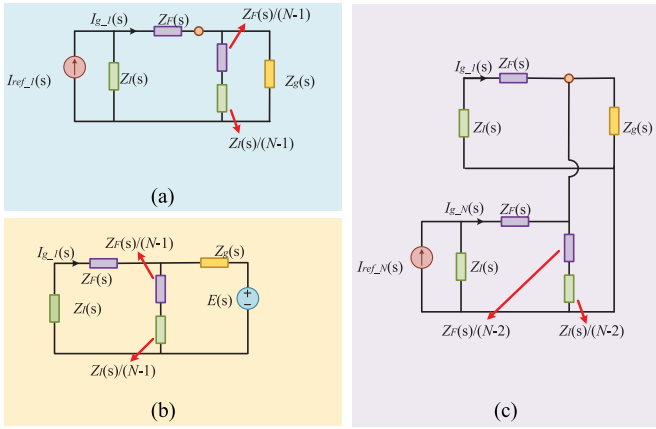

Fig. 5. SAPF #1 stimulated by three sources.

feedback control. The grid is described by grid EMF $E(s)$ and grid impedance $Z_g(s)$.

Based on the equivalent model and the superposition theorem, the output current $I_g(s)$ of a single SAPF can be written

$$I_g(s) = \frac{Z_I(s)I_{\text{ref}}(s) - E(s)}{Z_I(s) + Z_F(s) + Z_g(s)}. \tag{2}$$

$Z_I(s)$ and $Z_F(s)$ can be obtained by solving (1) and (2)

$$Z_I(s) = \frac{\text{PIR}(s)G_{\text{delay}}(s)}{s^2L_1C_1 + sC_1\text{PIR}(s)G_{\text{delay}}(s) - G_{\text{delay}}(s) + 1} \tag{3}$$

$$Z_F(s) = \frac{s^3L_1C_1L_2 + s(L_1+L_2) + s^2C_1L_2\text{PIR}(s)G_{\text{delay}}(s)}{s^2L_1C_1 + sC_1\text{PIR}(s)G_{\text{delay}}(s) - G_{\text{delay}}(s) + 1}. \tag{4}$$

B. Modeling of Parallel Three-Level SAPF System

Based on the model derived for a single three-level SAPF, the structure and model of the modular SAPF system can be obtained as shown in Fig. 4. Each SAPF module has an independent controller, dc bus, and *LCL* output filter. For example, the transfer function of SAPF #1 can be obtained using Kirchhoff's current law and the superposition theorem as

$$I_{g\_1}(s) = G_P(s)I_{\text{ref}\_1}(s) + \sum_{n=2}^{N} G_N(s)I_{\text{ref}\_n}(s) + G_E(s)E(s) \tag{5}$$

where N is the number of parallel units. There are three components in (5) denoting three stimulating sources from the modular system, which are: current reference of SAPF #1 represented by I_{ref_1}, current references of other parallel SAPF represented by I_{ref_n}, and grid voltage represent by $E(s)$. $G_P(s)$, $G_N(s)$ and $G_E(s)$ represent transfer functions of these three stimulating sources to $I_{g\_1}(s)$, respectively.

Fig. 5 shows the equivalent circuits when SAPF 1# is excited by the three different sources mentioned. According to the superposition theorem, these three can be treated separately as shown in Fig. 5(a)–(c). Fig. 5(a) is the equivalent circuit model excited by I_{ref_1}. The remaining $(N-1)$ SAPFs are treated as $(N-1)$ impedances in parallel: $Z_F(s)/(N-1)$ and $Z_I(s)/(N-1)$. Fig. 5(b) shows the equivalent circuit model excited by $E(s)$, wherein, all SAPF are regarded as impedances. Finally, Fig. 5(c) shows the equivalent model excited by $I_{\text{ref\_N}}$. The impedance of remaining $(N-2)$ parallel inverters is $Z_F(s)/(N-2)$ and $Z_I(s)/(N-2)$.

From the equivalent circuits shown in Fig. 5, $G_P(s)$, $G_N(s)$, and $G_E(s)$ are derived as following:

$$G_P(s) = \frac{Z_I(s)[Z_I(s) + Z_F(s) + (N-1)Z_g(s)]}{[Z_I(s) + Z_F(s)][Z_I(s) + Z_F(s) + NZ_g(s)]} \tag{6}$$

$$G_N(s) = \frac{-Z_I(s)Z_g(s)}{[Z_I(s) + Z_F(s)][Z_I(s) + Z_F(s) + NZ_g(s)]} \tag{7}$$

$$G_E(s) = \frac{-1}{Z_I(s) + Z_F(s) + NZ_g(s)}. \tag{8}$$

If each SAPF has the same output current, we obtain

$$I_{\text{ref}\_1}(s) = I_{\text{ref}\_2}(s) = \cdots = I_{\text{ref}\_n}(s) \tag{9}$$

$$\begin{aligned} I_{g\_1}(s) &= \\ &G_P(s)I_{\text{ref}\_1}(s) + (N-1)G_N(s)I_{\text{ref}\_n}(s) + G_E(s)E(s) \\ &= \frac{Z_I(s)I_{\text{ref}\_1}(s) - E(s)}{Z_I(s) + Z_F(s) + NZ_g(s)}. \end{aligned} \tag{10}$$

Comparing (10) against (2), it can be found that for a specific SAPF, such as aforementioned SAPF #1, the increase in the number of SAPF connected in parallel causes the equivalent grid impedance to increase by N times. This can be confirmed readily by the modeling circuit in Fig. 6. Given same parameters for *LCL* filter and control algorithm, the output impedance $Z_F(s)$ of every SAPF module is the same. Each SAPF module is connected at the point of common coupling (PCC) with grid impedance $Z_g(s)$. As shown in Fig. 6(b), $Z_g(s)$ can be treated as N fractions of $N \cdot Z_g(s)$ in parallel. Since output current of each SAPF is the same, PCC can be shifted to the right as shown in Fig. 6(c). $Z_F(s)$ and $N \cdot Z_g(s)$ are then connected in series as shown in Fig. 6(c). Thus, it can be clearly shown that the equivalent grid impedance of N parallel SAPF systems is increased by N times.

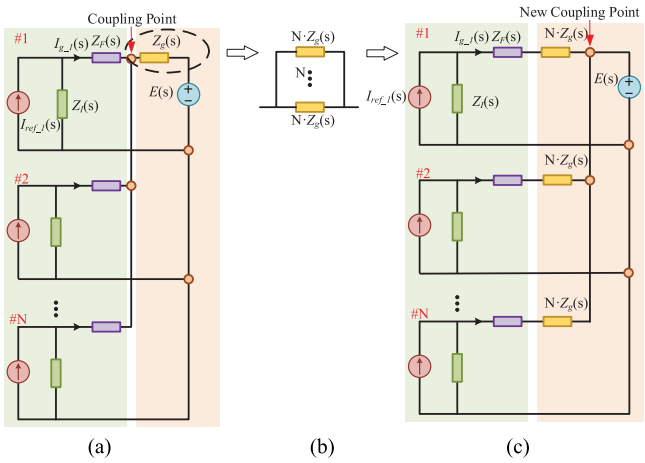

Fig. 6. Modeling of modular SAPF.

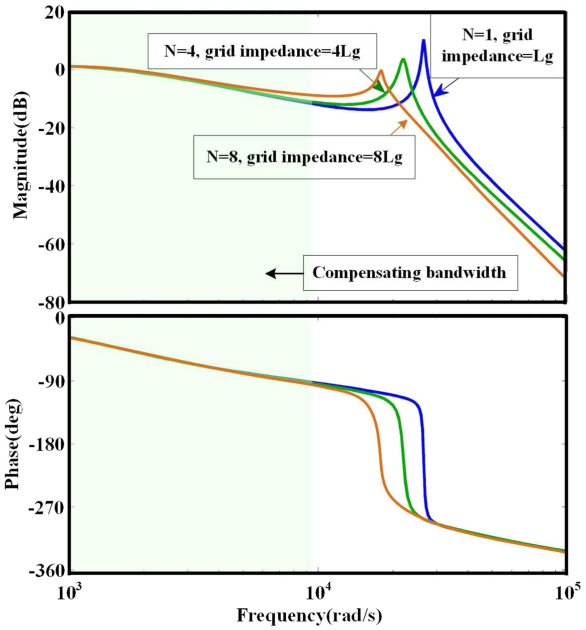

Fig. 7. Bode diagram of $I_g(s)/I_{\text{ref}}(s)$ with different grid impedance.

Given the discussion above, it is explicit to understand that the resonant peak of the transfer function of a SAPF module shifts toward left when the number of paralleled SAPF increases as shown by the Bode plot in Fig. 7. The phase plot in Fig. 7 shows that system stability margin decreases with increased N, which poses a greater challenge to the control bandwidth margin and resonance suppression of conventional modular SAPF.

Unlike sine wave grid-tied inverters, SAPF injects high-frequency harmonic current ranging from 150 to 1500 Hz as shown by the shaded area in Fig. 7, rather than the fundamental sine wave component. For the conventional modular SAPF, as the frequency of resonant peak decreases while the number of modules N increases, the frequency band of compensating current will come very close to the resonant peak. The stability margin also drops and resonance tends to occur. Moreover, it can also be seen from Fig. 7 that the control bandwidth is no longer sufficient for high order harmonics compensation for an increased N. Finally, in the conventional modular SAPF with the same filter inductance and control parameters, a tradeoff between the dynamic response and the stability control is difficult to obtain either by passive components design or by active damping control. This is the challenge that the present effort aims to fundamentally address.

III. *LCL* Filter Design, Resonance Analysis, and Self-Adaptive Active Damping for Hybrid Modular Three-Level SAPF

Based on the generalized modeling of modular SAPF and understanding of their limitations, a novel hybrid modular three-level SAPF is proposed in this paper. The hybrid system combines larger capacity modules and smaller modules. Larger capacity modules have higher *LCL* filter values and lower switching frequency while smaller capacity modules have lower *LCL* filter values and higher switching frequency. The design aims to compensate the lower order harmonics and higher order harmonics individually. In the proposed hybrid system, the conventional SAPF compensating band as shown in Fig. 7 is divided into high and low order bands. Such a design using different *LCL* filter parameters for two compensating bands allows more room to achieve tradeoff between the dynamic response and the system stability control. Next, a modular SAPF *LCL* filter design method and a modular system resonance analysis will be presented, followed by a novel self-adaptive active damping strategy for hybrid modular SAPF.

A. *LCL Design of Modular SAPF*

Given the modular SAPF capabilities and limitations revealed in Section II, a design method for the SAPF passive filter must be developed. A step-by-step procedure to design the *LCL* filter for a modular SAPF is proposed as follows:

1) First the inverter side inductance L_1 is designed in order to limit the current ripple generated by the SAPF within 10% rated compensating current [26], [27].
2) The acceptable level of the reactive power to be absorbed by the filter capacitor under rated conditions is selected, and this determines the capacitor value [26].
3) The overall inductance of inductors installed should be limited to well below the 10% of the base impedance.
4) As shown from the modeling analysis in Section II, the equivalent grid side inductance changes with the parallel number of modules.
5) Minimize the filter volume by using lower inductances and higher capacitances. This is due to the fact that SAPF compensating current causes higher voltage drop than the grid tied inverter.
6) The resonance point should be higher than that for the sine wave grid-tied inverters because SAPF's compensating band is wider.
7) Last the current variation rate generated by the SAPF should be greater than the expected current. This can be

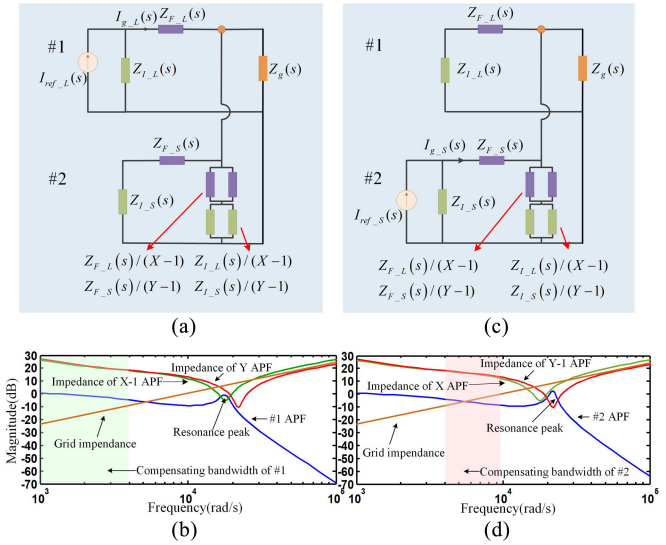

Fig. 8. Equivalent circuit and bode diagram of the hybrid parallel SAPF.

expressed by:

$$L < \frac{U_{\rm dc} - 1.1U_g}{I_c} \tag{11}$$

where $U_{\rm dc}$ and I_c are the SAPF dc link voltage and compensating current, respectively, which imposes another limitation to the converter side inductance.

B. Resonance and Stability Analysis of Hybrid Modular Three-Level SAPF

To investigate the tracking and resonance issues among modules of different capacities, simplified equivalent circuit models can be derived from Fig. 5. Fig. 8(a) shows a simplified model for the larger SAPF module #1 and Fig. 8(c) shows simplified model for the smaller SAPF module #2.

In Fig. 8(a) and (c), X represents the number of larger capacity modules and Y represents the number of smaller capacity modules. The #1 and #2 converters stand for one larger and one smaller capacity modules, respectively. The other $(X-1)$ larger capacity modules and $(Y-1)$ smaller capacity modules can be simplified as impedances. Based on this simplification, we can get the bode diagram of $I_{g\_L}(s)/I_{\rm ref\_L}(s)$ shown in Fig. 8(b), where $(X-1)$ larger capacity module impedance, Y smaller capacity module impedance, and grid impedance are plotted. The compensating current of #1 SAPF with a bandwidth ranging from 150 to 650 Hz is divided by the impedance of the grid, $(X-1)$ SAPF with larger capacity and Y SAPF with lower capacity. It can be observed that within the compensating band under 13th order, grid impedance is much smaller than the impedance of $(X-1)$ SAPF and Y SAPF. The compensating current is mainly injected into the grid. It is clearly shown that the compensating current band of SAPF #1 is far from the resonance peak and provides sufficient control bandwidth. Therefore, it allows more space to tradeoff between the compensating dynamic response and stability control.

For SAPF #2, the smaller capacity module injects compensating harmonics higher than the 13th order, i.e., from 650 Hz onwards. As shown in Fig. 8(d), the Bode diagram of $I_{g\_S}(s)/I_{\rm ref\_S}(s)$ shows that smaller *LCL* parameters design push the resonant peak higher and creates sufficient control bandwidth for high order compensating current. In contrast to the conventional modular SAPF in Fig. 7, Fig. 8(d) shows that the modular SAPF enables greater margin and bandwidth to tradeoff between dynamic response and stability control. Moreover, the higher switching frequency and low inductance further improve the current tracking response ability. According to the compensating band for SAPF #2, the grid impedance is relatively large, but X SAPF is designed with higher *LCL* parameters. Therefore, grid impedance is still much smaller than the impedance of X SAPF. Further, the higher order harmonic components are usually smaller in magnitude, and hence, fewer lower capacity modules, possibly one or two, is required. In short, it can be concluded that the compensating current mainly flows into the grid.

It should be noted that in the hybrid system proposed in this paper, the dynamic response and the stability control are not only balanced by passive filter design, but also controlled by active damping. Therefore, the resonance does not need to be suppressed further by the controller gain regulation as that in [14] and [15] which compromises current tracking precision.

In this paper, to achieve fast current dynamic response and salient stability control, a novel self-adaptive resonance suppressing strategy is then proposed for the hybrid paralleled system.

C. Limitations Analysis of Conventional Resonance Damping Methods and the Novel Self-Adaptive Active Damping for Hybrid Modular Three-Level SAPF

Although *LCL* filters can better meet grid interconnection standards with significantly smaller size and cost, they also trigger resonance between the inverter and the grid. An active or a passive damping measure is usually adopted to suppress possible resonances. In case of modular SAPFs, an active damping method produces better results.

The active damping method proposed in [27] is widely used in the grid-tied inverter, which introduces the capacitor branch current as the feedback quantity to enhance the damping effect of the system. However, in the method described in [27], the damping feedback control coefficient *K* is fixed neglecting the grid side impedance, and the converter side inductance may vary. Consider the example where the converter side inductance varies, if K is always fixed when the inductance lowers due to the change in load current, the system stability margin shrinks as shown in Fig. 9(a). As shown in Fig. 9(b), with an increased number of modules N in parallel, grid impedance grows to $N \cdot L_g$. The resonant frequency of the SAPF system shifts toward the left and the stability margin of the SAPF system decreases.

As shown from the modular SAPF modeling, the equivalent grid impedance varies widely due to the number of modules connected. Furthermore, the converter side inductance also changes dramatically due to the high crest factor of compensating

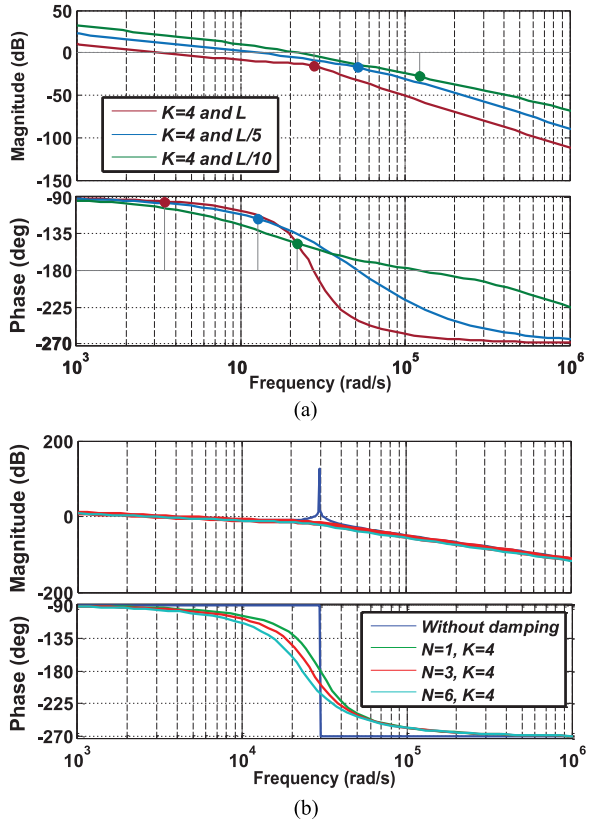

Fig. 9. (a) Frequency characteristics with different output current. (b) Frequency characteristics with different number of parallel units.

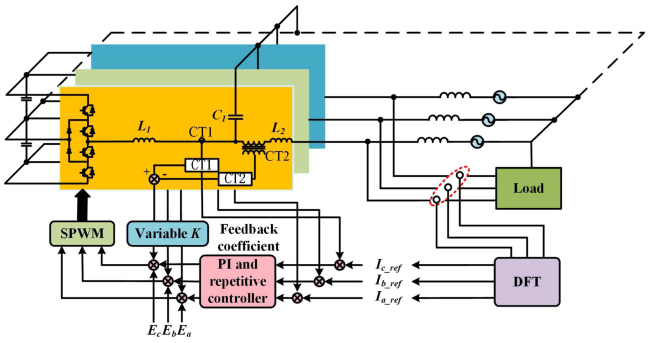

Fig. 10. Controller design with proposed self-adaptive active damping.

current in contrast to conventional sine wave inverter. Therefore, the method in [27] cannot be directly employed. Instead, we proposes a novel self-adaptive active damping for the hybrid SAPF. In this method, K is not fixed but obtained through optimization on the modules number, and more importantly, the instant inductance determined by the compensating current.

The novel self-adaptive active damping method based on capacitor branch current feedback for the hybrid modular three-level SAPF is shown in Fig. 10. The new strategy features a variable active damping coefficient K' for different values of N and different values of compensating current. Its corresponding control diagram is shown in Fig. 11.

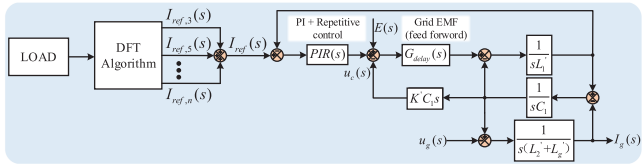

Fig. 11. Novel self-adaptive active damping strategy.

In this paper, only the inductor current tracking reference is discussed, $E(s)$ representing the grid voltage behaves as a disturbance and is considered to be zero when analyzing the resonance and stability of hybrid modular three-level SAPF. Therefore, neglecting $E(s)$ and the effect of $G_{\text{delay}}(s)$, the open loop transfer function of the system can be given by

$$\begin{aligned} G_{gc}(s) &= \frac{I_g(s)}{u_c(s)} \\ &= \frac{1}{L_1'(L_2'+L_g')C_1 s^3 + K'(L_2'+L_g')C_1 s^2 + (L_1'+L_2'+L_g')s} \end{aligned} \tag{12}$$

where K' is the variable feedback coefficient, L_1', L_2' are the real inductance as a function of the output current, and L_g' is the equivalent grid impedance of one SAPF in the hybrid parallel SAPF, and can be calculated by the hybrid equivalent circuit in Fig. 8.

To simplify the discussion, $G_{gc}(s)$ can be rewritten as the product of an integral loop and a second order oscillation loop:

$$G_{gc}(s) = \frac{1}{L_1'(L_2'+L_g')C_1 s} \frac{1}{s^2 + K's/L_1' + \omega_{\text{res}}^2} \tag{13}$$

where ω_{res} is the resonance frequency of the second order oscillation loop

$$\omega_{\text{res}}^2 = \frac{L_1' + L_2' + L_g'}{L_1'(L_2' + L_g')C_1}. \tag{14}$$

According to the definition of damping ratio ξ in the second-order oscillation loop, it can be given as

$$\xi = \frac{K'}{2L_1'\omega_{\text{res}}}. \tag{15}$$

In the underdamped second-order oscillation loop, given a decrease in ξ, the overshoot increases and the response time decreases. On the other side, with the increase of ξ, the overshoot decreases, but the system response slows down. According to the control theory, when damping ratio equals to 0.707, the system overshoot is moderate and the regulation time is short, where the system is at the best damping condition. In SAPF applications, at the point of $\xi = 0.707$, the hybrid SAPF system can reach an optimal tradeoff between resonance suppression and time response. Therefore, the optimum damping ratio of the second order oscillation loop is chosen as $\xi = 0.707$.

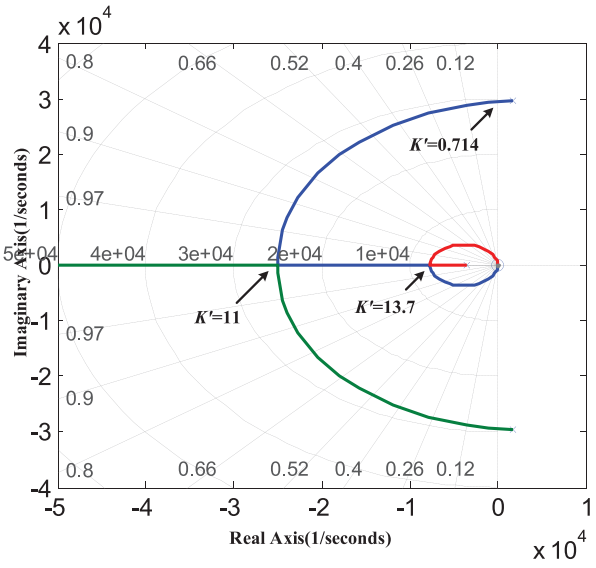

Fig. 12. Generalized root locus of (12) with different K'.

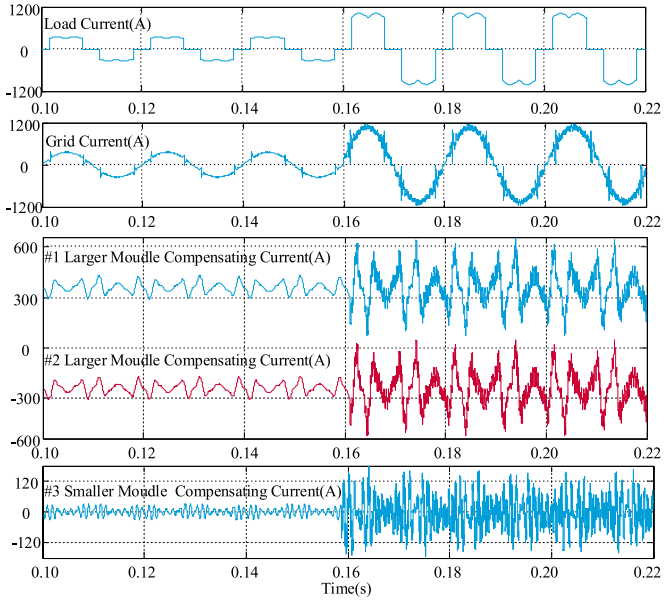

Fig. 13. Simulation results of output current increase with three SAPF in parallel operation.

Take $\xi = 0.707$ and substitute (14) into (15), we can attain the expression of the optimized feedback coefficient K'

$$K' = \sqrt{\frac{2L_1'(L_1' + L_2' + L_g')}{(L_2' + L_g')C_1}}. \tag{16}$$

Further analysis of Fig. 11 indicates that the system stability is primarily determined by the feedback coefficient K'. Fig. 12 shows the generalized root locus of (12) with different K'. The stable range of K' is from 0.714 to 11. Therefore, in our system, to ensure K' calculated by (16) is in a reasonable range, we constrain the feedback coefficient K' as follows:

$$K' = \begin{cases} 0.714, & K' < 0.714 \\ \sqrt{\frac{2L_1'(L_1' + L_2' + L_g')}{(L_2' + L_g')C_1}}, & 0.714 < K' < 11 \\ 11, & 11 < K'. \end{cases} \tag{17}$$

The proposed novel self-adaptive active damping control method for the hybrid modular three-level SAPF can be used not only in industrial applications where variable loads are connected to the system, but also, the scenarios where there is interaction of multiple SAPF systems connected to a weak power grid, and an increased stability margin is required for the stability of SAPF system.

IV. Simulation and Experimental Results

A. Simulation Results

Influence of the inductance and the change in the module number on the system stability margin is illustrated in Fig. 9 with a constant damping feedback coefficient K. In order to interpret it explicitly, we carry out two simulations in MATLAB/Simulink.

Fig. 13 shows the simulation results for three SAPFs in parallel operation with the load current tripled at $t = 0.16$ s. The filter inductance is adjusted according to the change of the output current at $t = 0.16$ s, while the feedback coefficient K of active damping is kept constant. We can see from the results that before $t = 0.16$ s, the hybrid SAPF system with two larger units and one smaller units compensates the harmonics well. The load current and output currents tripled at $t = 0.16$ s, and therefore the inductance decreases. However, due to the unchanged feedback coefficient K, resonance occurs in the system. This is in accordance with the decrease in stability margin in Fig. 9(a).

In Fig. 14, the operating condition is the same as described in Fig. 13 before $t = 0.16$ s except that the inductance is set as a constant value. After $t = 0.16$ s, load current doubles and we turn ON another three SAPF units, which means that the parallel units number N increases from 3 to 6. System resonance occurs similarly because of the unchanged K. The simulation results again match the conclusions derived from Fig. 9(b).

B. Experimental Results

The hybrid SAPF system as shown in Fig. 15 is also implemented to verify the proposed design and resonance suppression strategy. The larger module power rating is fixed at 100 A aiming to compensate the low-order harmonics less than 13th order, and the smaller 50-A module compensating the high order harmonics higher than 13th order. The main parameters are listed in Table I.

The main circuits are shown in Fig. 16. A 100-A Infineon three-level power module F3L100R07W2E3 is chosen for 50-A smaller module. Two F3L100R07W2E3 are connected in parallel to serve as the 100-A larger power module as shown in Fig. 16(b).

Figs. 17 and 18 show the self-adaptive damping test results. In Fig. 17, Channels 1 and 5 are load current and grid current, respectively. Before $t = 32$ ms, #2 SAPF (100 A) and #3 SAPF (50A) are in stable operation using traditional active

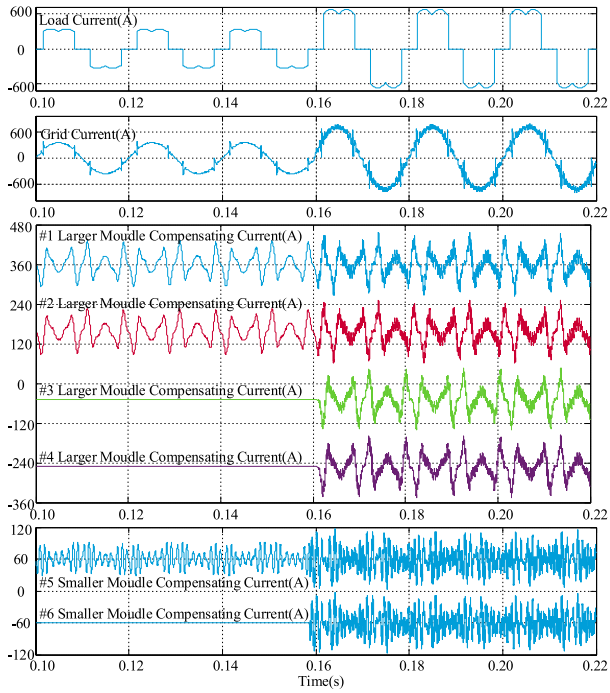

Fig. 14. Simulation results of parallel units increase with six SAPF in parallel operation.

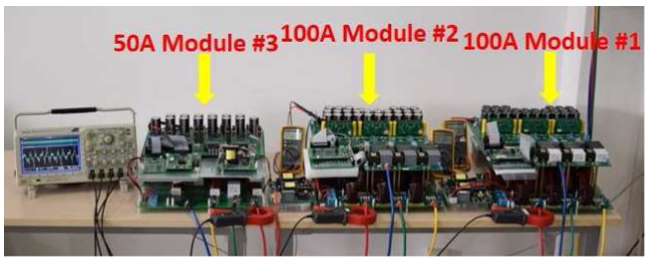

Fig. 15. Hybrid modular three-level SAPF prototype.

TABLE I
PROTOTYPE AND THE EXPERIMENTAL PARAMETERS

Item	Value
Grid frequency	50 Hz
Switching frequency (100 A, 50 A)	20 kHz, 40 kHz
Phase voltage (RMS)	230 V
DC voltage	800 V
100-A module *LCL*	800/4 μH, 20 μF, 75 μH
50-A module *LCL*	200/2 μH, 10 μF, 50 μH
IGBT module	F3L100R07W2E3

damping method as shown by Channels 2, 3, and 4. At $t = 32$ ms, #1 SAPF (100 A) starts its operation as shown by Channel 2 using traditional active damping method. It can be observed from the waveforms that the traditional active damping method with a fixed damping feedback coefficient fails to effectively suppress resonance because the number of parallel modules N changes. After $t = 64$ ms, the modular system starts to operate with the proposed self-adaptive active damping method, and the resonance is well suppressed.

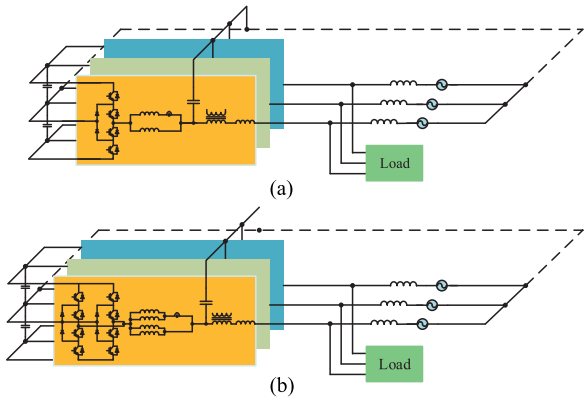

Fig. 16. (a) 50-A module topology. (b) 100-A module topology.

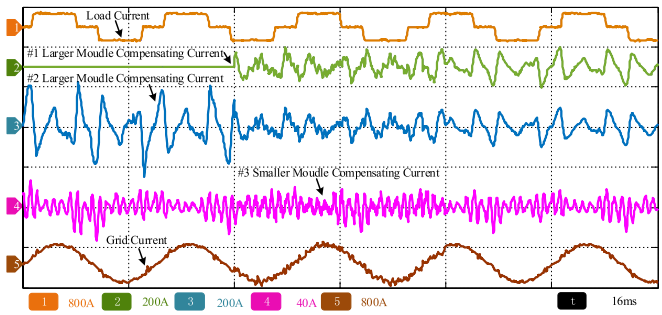

Fig. 17. Compensating current of hybrid modules with different damping methods.

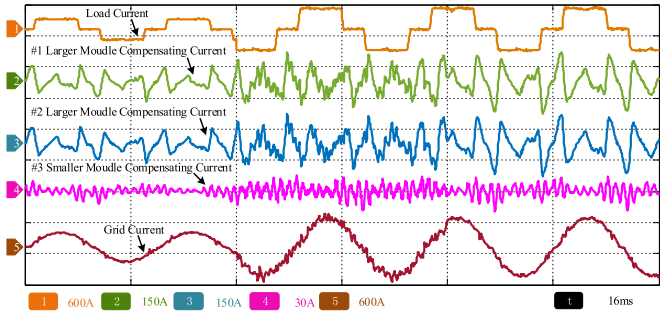

Fig. 18. Compensating current of hybrid modules with load change.

Fig. 18 shows the test results with a change in load current. Channels 2, 3, and 4 show the compensating currents of #1 SAPF(100 A), #2 SAPF(100 A), #3 SAPF(50 A), which are stable before $t = 32$ ms using traditional active damping. However, with load doubled at $t = 32$ ms, resonance starts to appear in modular system. At $t = 64$ ms, the proposed self-adaptive active damping is applied to the system and resonance disappears. This is because the feedback coefficient now varies with change in load current. Therefore, the resonance is suppressed, rendering the system stable.

It can be concluded from Figs. 17 and 18 that with a fixed feedback coefficient K, resonance occurs when inductance or parallel number N change. These experiment results are

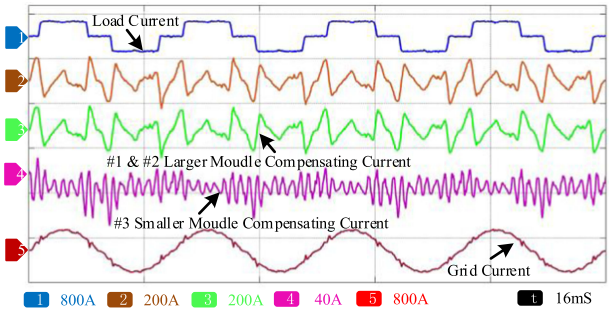

(a)

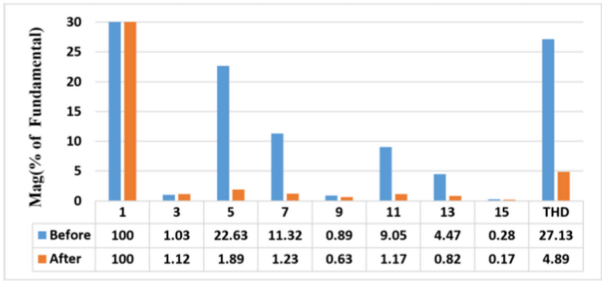

	1	3	5	7	9	11	13	15	THD
Before	100	1.03	22.63	11.32	0.89	9.05	4.47	0.28	27.13
After	100	1.12	1.89	1.23	0.63	1.17	0.82	0.17	4.89

(b)

Fig. 19. (a) Experimental results of three SAPF in parallel. (b) THD of grid current.

consistent with the analysis in Fig. 9 and the simulation results in Figs. 13 and 14.

Fig. 19 shows the compensating currents of 50-A module and 100-A modules in parallel using the self-adaptive damping technique together with the spectrum of grid current before and after compensation. From Channel 1 to 5 are: 1) the load current; 2) modules #1 and #2 (100 A) compensating current; 3) module #3 (50 A) compensating current, and 4) the grid current after compensation. This result shows that the 50-A module has fast dynamic response since it has lower *LCL* parameters and higher switching frequency. The THD of grid current is 27.13% before the compensation and 4.89% after.

V. Conclusion

This paper improves upon the conventional modular SAPF mathematical models to investigate tradeoffs between dynamic response and stability control. According to the analysis results obtained from the model, a novel hybrid modular three-level SAPF structure is proposed. In contrast to previous methods, the proposed system is composed of two modules, each with different current carrying capacities, *LCL* filter parameters, and switching frequencies. Finally, a novel self-adaptive resonance suppression strategy is proposed to take into account the variations in the number of modules and load current. Theoretical analysis and experimental results confirm that the hybrid modular SAPF and its self-adaptive resonance suppression strategy can achieve a better tradeoff between dynamic response and stability control as compared with the conventional modular SAPF. The proposed system may be used in industrial applications, in particular for power quality improvement in weak power grids.

References

[1] J. Fang, G. Xiao, X. Yang, and Y. Tang, "Parameter design of a novel series-parallel-resonant LCL filter for single-phase half-bridge active power filters," *IEEE Trans. Power Electron.*, vol. 32, no. 1, pp. 200–217, Jan. 2017.

[2] J. C. Alfonso-Gil, E. Pérez, C. Arino, and H. Beltran, "Optimization algorithm for selective compensation in a shunt active power filter," *IEEE Trans. Ind. Electron.*, vol. 62, no. 6, pp. 3351–3361, Jun. 2015.

[3] M. Angulo, D. A. Ruiz-Caballero, J. Lago, M. L. Heldwein, and S. A. Mussa, "Active power filter control strategy with implicit closed-loop current control and resonant controller," *IEEE Trans. Ind. Electron.*, vol. 60, no. 7, pp. 2721–2730, Jul. 2013.

[4] J. He, Y. W. Li, and F. Blaabjerg, "Flexible microgrid power quality enhancement using adaptive hybrid voltage and current controller," *IEEE Trans. Ind. Electron.*, vol. 61, no. 6, pp. 2784–2794, Jun. 2014.

[5] P. Acuna, L. Morán, M. Rivera, J. Dixon, and J. Rodriguez, "Improved active power filter performance for renewable power generation systems," *IEEE Trans. Power Electron.*, vol. 29, no. 2, pp. 687–694, Feb. 2014.

[6] H. Yi *et al.*, "A source-current-detected shunt active power filter control scheme based on vector resonant controller," *IEEE Trans. Ind. Appl.*, vol. 50, no. 3, pp. 1953–1965, May/Jun. 2014.

[7] R. Dian, W. Xu, and C. Mu, "Improved negative sequence current detection and control strategy for H-bridge three-level active power filter," *IEEE Trans. Appl. Supercond.*, vol. 26, no. 7, pp. 1–5, Oct. 2016, Art. no. 0611905.

[8] S. Rahmani, N. Mendalek, and K. Al-Haddad, "Experimental design of a nonlinear control technique for three-phase shunt active power filter," *IEEE Trans. Ind. Electron.*, vol. 57, no. 10, pp. 3364–3375, Oct. 2010.

[9] Z. Wang, C. Xie, C. He, and G. Chen, "A waveform control technique for high power shunt active power filter based on repetitive control algorithm," in *Proc. 25th Annu. IEEE Appl. Power Electron. Conf. Expo.*, 2010, pp. 361–366.

[10] Y. Tang, P. C. Loh, P. Wang, F. H. Choo, F. Gao, and F. Blaabjerg, "Generalized design of high performance shunt active power filter with output lcl filter," *IEEE Trans. Ind. Electron.*, vol. 59, no. 3, pp. 1443–1452, Mar. 2012.

[11] R. E. Shatshat, M. Salama, and M. Kazerani, "Artificial intelligent controller for current source converter-based modular active power filters," *IEEE Trans. Power Del.*, vol. 19, no. 3, pp. 1314–1320, Jul. 2004.

[12] J. Ju, D. Xu, M. Chen, J. Xu, B. Shen, and F. Zhang, "Control strategy of multi-modular active power filter system," in *Proc. 22nd Annu. Appl. Power Electron. Conf. Expo.*, Feb. 2007, pp. 686–691.

[13] L. Asiminoaei, C. Lascu, F. Blaabjerg, and I. Boldea, "Performance improvement of shunt active power filter with dual parallel topology," *IEEE Trans. Power Electron.*, vol. 22, no. 1, pp. 247–259, Jan. 2007.

[14] Y. Wang, Q. Xu, and G. Chen, "Simplified multi-modular shunt active power filter system and its modelling," *IET Power Electron.*, vol. 8, no. 6, pp. 967–976, 2015.

[15] P. Dang, T. Ellinger, and J. Petzoldt, "Dynamic interaction analysis of APF systems," *IEEE Trans. Ind. Electron.*, vol. 61, no. 61, pp. 4467–4473, Sep. 2014.

[16] J. H. R. Enslin and P. J. M. Heskes, "Harmonic interaction between a large number of distributed power inverters and the distribution network," *IEEE Trans. Power Electron.*, vol. 4, no. 6, pp. 1586–1593, Nov. 2004.

[17] J. L. Agorreta, M. Borrega, J. López, and L. Marroyo, "Modeling and control of-paralleled grid-connected inverters with LCL filter coupled due to grid impedance in PV plants," *IEEE Trans. Power Electron.*, vol. 26, no. 3, pp. 770–785, Mar. 2011.

[18] Y. Zhang and H. Ma, "Theoretical and experimental investigation of networked control for parallel operation of inverters," *IEEE Trans. Ind. Electron.*, vol. 59, no. 4, pp. 1961–1970, Apr. 2012.

[19] M. Lu, X. Wang, P. Loh, and F. Blaabjerg, "Resonance interaction of multi-parallel grid-connected inverters with LCL filter," *IEEE Trans. Power Electron.*, vol. 32, no. 2, pp. 894–899, Feb. 2017.

[20] W. Wu, Y. He, T. Tang, and F. Blaabjerg, "A new design method for the passive damped LCL and LLCL filter-based single-phase grid-tied inverter," *IEEE Trans. Ind. Electron.*, vol. 60, no. 10, pp. 4339–4350, Oct. 2013.

[21] J. He, Y. W. Li, D. Bosnjak, and B. Harris, "Investigation and active damping of multiple resonances in a parallel-inverter-based microgrid," *IEEE Trans. Power Electron.*, vol. 28, no. 1, pp. 234–246, Jan. 2013.

[22] M. Lu, X. Wang, F. Blaabjerg, S. Muyeen, A. Al-Durra, and S. Leng, "Grid-voltage-feedforward active damping for grid-connected inverter with lcl filter," in *Proc. 2016 IEEE Appl. Power Electron. Conf. Expo.*, 2016, pp. 1941–1946.

[23] D. G. Holmes, T. A. Lipo, B. P. McGrath, and W. Y. Kong, "Optimized design of stationary frame three phase ac current regulators," *IEEE Trans. Power Electron.*, vol. 24, no. 11, pp. 2417–2426, Nov. 2009.
[24] J. Sun, "Small-signal methods for ac distributed power systems a review," *IEEE Trans. Power Electron.*, vol. 24, no. 11, pp. 2545–2554, Nov. 2009.
[25] C. Yu *et al.*, "Modeling and resonance analysis of multi-parallel inverters system under asynchronous carriers conditions," *IEEE Trans. Power Electron.*, vol. 32, no. 4, pp. 3192–3205, Apr. 2017.
[26] M. Liserre, F. Blaabjerg, and S. Hansen, "Design and control of an LCL-filter-based three-phase active rectifier," in *Proc. 36th IAS Annu. Meet. Conf. Rec. Ind. Appl. Conf.*, 2001, pp. 299–307.
[27] E. Twining and D. G. Holmes, "Grid current regulation of a three-phase voltage source inverter with an LCL input filter," *IEEE Trans. Power Electron.*, vol. 18, no. 3, pp. 888–895, May 2003.

Yong Wang (M'12) received Ph.D. degree in power electronics from Zhejiang university, Hangzhou, China, in 2005.

From 2005 to 2008, he was a Senior Researcher in Samsung Advanced Institute of Technology, Suwon, South Korea, working on the fuel cell grid-tied inverter. From 2008 to 2010, he was working in Danfoss, Soenderborg, Denmark, as a power electronics Hardware Engineer. In the year 2010, he joined Shanghai Jiao Tong University, Shanghai, China, where he is currently an Associate Professor in the Department of Electrical Engineering. His main research interests include active power filter, multilevel conversion technology, grid-tied inverter, LLC, and so on.

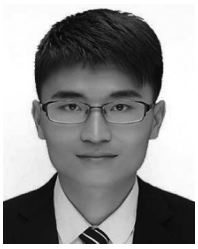

Jialong Xu was born in 1993. He received the B.S. degree in electrical engineering and automation from Northwestern Polytechnical University, Xi'an, China, in 2015. He is currently working toward the M.S. degree in electrical engineering at Shanghai Jiao Tong University, Shanghai, China.

His current research interests include power quality problems and multilevel convertors.

Ling Feng (S'17) was born in 1991. He received the B.Sc. and M.Sc. degrees in electrical engineering from Shanghai Jiao Tong University, Shanghai, China, in 2014 and 2017, respectively.

His current research interests include power quality problems and multilevel convertors.

Chengmin Wang was born in 1970. He received the Ph.D. degree in power system from the Harbin Institute of Technology, Harbin, China, in 2002.

He is currently a Full Professor at Shanghai Jiao Tong University, Shanghai, China. He has been involved in studying renewable energy system, power system stability, electricity market, etc., since 1996. He has published more than 100 journal articles and books, in which there are more than 40 papers indexed by SCI or EI.